Applied Catalysis B: Environmental 218 (2017) 506–514

Contents lists available at ScienceDirect

Applied Catalysis B: Environmental

journal homepage: www.elsevier.com/locate/apcatb

Ultrasmall gold nanoparticles confined in zeolite Y: Preparation and activity in CO oxidation

Yi-Hsiu Chen [a], Chung-Yuan Mou [b], Ben-Zu Wan [a,*]

[a] Department of Chemical Engineering, National Taiwan University, Taipei 106, Taiwan
[b] Department of Chemistry, National Taiwan University, Taipei 106, Taiwan

ARTICLE INFO

Article history:
Received 26 January 2017
Received in revised form 2 June 2017
Accepted 27 June 2017
Available online 28 June 2017

Keyword:
Proton-type zeolite Y (HY)
Surface charge
Surface modification
Gold catalyst
CO oxidation

ABSTRACT

In this study, proton-type zeolites Y (HY) with Al/Si ratio of 0.36 were used as a support for deposition of $HAuCl_4$ (in pH 6 solution) to prepare Au/Y catalysts for CO oxidation at 25 °C. The low isoelectric point of HY (~pH = 2) made this support inappropriate for loading negatively charged gold complexes, and caused the generation of large gold particles with low catalytic activity. We found that through a Na^+ pretreatment of HY to form H(Na)Y, the surface charge can be reversed to positive, thus favoring the deposition. The resulting Au/H(Na)Y, without any high temperature treatment, gave excellent activity in CO oxidation comparable to Au/TiO_2. The CO oxidation rate of 0.21 mol CO/mol Au·s remained stable at 25 °C. HRTEM images of the catalyst show highly dispersed gold nanoparticles ~1 nm confined in the nanocage of H(Na)Y. XPS spectra show high proportion of Au(III) associated with Au-O. The weak Au-O in Au/H(Na)Y is found responsible for the easy reduction in TPR. For comparison, the other alternative procedures of gold deposition were also tried to reverse the surface charge of HY by decreasing the pH of solution. However, high contents of residual Cl in the nano-gold catalyst lead to almost no activity in CO oxidation.

1. Introduction

Supported gold nanoparticle has been found capable of catalyzing many reactions with high activity and selectivity [1–5]. It attracted a lot of attentions because of its size-sensitivity in catalytic activities. Ultrasmall gold nanoparticle (or nanocluster) in the size ~1 nm is particularly interesting for its great promise in various reaction systems including oxidation, hydrogenation, C—C coupling, and photocatalysis [6,7].

However, most of the above promises are based on ligand-protected gold nanoclusters in solution [8]. Gas phase reactions catalyzed by supported ultrasmall gold nanoparticles are much less explored because of difficulties in their synthesis [9]. The low Tamman temperature of gold makes it easily aggregate to form larger particles, resulting in severe loss of activity [10]. It is very difficult to prepare stable supported ultrasmall gold nanoparticles with a high dispersion similar to that can be achieved with platinum group metals (~1 nm in size). Confining gold nanoparticles in porous materials is a viable approach to prevent their aggregation. Porous aluminosilicate materials, either with micropores [11–14] or mesopores (e.g., SBA-15 or MCM-41 [15,16]), has been used to encapsulate gold nanoparticles. However, the low isoelectric point (IEP) of aluminosilica (at *ca.* pH 2) makes $HAuCl_4$-derived gold complexes with negative charges difficult to deposit onto the supports. An elevated pH is necessary to hydrolyze chloroauric acid ($HAuCl_4$) to $Au(OH)_4^-$, making standard deposition methods not suitable because of the charge repulsion. Traditional preparation procedures like impregnation (IMP) and deposition-precipitation (DP) resulted in large gold particles sizes and low activity [15,17].

Researchers have tried deposition of gold species onto supports at the pH close to IEP of the supports [18,19]. However, the residual chlorides on the prepared catalysts could cause deactivation in CO oxidation [20]. Alternatively, surface modification of mesoporous aluminosilicate materials with aminosilanes [15,16,21–25] can lead to a better dispersion. In a specially designed method, Iglesia and coworker were able to make gold nanoparticle encapsulated in microporous zeolite LTA by using the mercaptosilane MPTMS (3-mercaptopropyl-trimethoxysilane) as a simultaneous encapsulating and structure-directing agent. However, removing the organics by calcination at high temperature still cause size growths of gold to ~2 nm (bigger than the cage of LTA) [26].

A promising approach for modifying surface charges of microporous aluminosilicate materials would be through modifying with small cations to reverse the charge of the support to positive. In our

* Corresponding author.
E-mail address: benzuwan@ntu.edu.tw (B.-Z. Wan).

http://dx.doi.org/10.1016/j.apcatb.2017.06.083
0926-3373/

previous work, a prior surface modification of proton-type zeolite Y (HY) by immersing in sodium salt solutions has been found to give excellent dispersion of gold and to improve the catalytic activity of the prepared Au/Y [27]. Further investigations on its surface charge found that this Na^+-treatment can reverse the zeta potential of HY to a positive value [28] in the solution close to neutral. The resulting positive-charge H(Na)Y zeolite can thus attract more negative gold species onto the supports.

The aim of this study is to investigate the effect of surface charge of HY on the supported gold nanoparticles. Other approach to reverse the surface charge of HY was done by lowering the pH (i.e., lower than 3) when preparing Au/Y [18]. We used AA to investigate the effect of surface charge on bulk Au loading and found that higher amounts of gold can be loaded onto supports when the surface charge of HY was reversed to positive. Meanwhile, fine dispersion of ultrasmall gold nanoparticle confined in the supercage of zeolite Y (~1 nm) was found. Various characterization techniques (AA, ICP-MAS and XPS) were used to determine the atomic composition of bulk and exterior regions of Au/Y. It is found that ultrasmall gold nanoparticle on modified HY (*i.e.*, Au/H(Na)Y in this study) are distributed closer to external surface, accompanied with high contents of Al species on the exterior surface. XANES, XPS and TPR were used to identify the residual Cl on each sample. High contents of Cl were indicated on the Au/Y prepared in acid conditions at low pH value. Catalytic CO oxidation tests on Au/H(Na)Y showed more stable and higher activity than that of Au/HY.

2. Experimental

2.1. Surface modification of HY zeolite

JRC-Z-HY5.3, from the Catalysis Society of Japan, is proton-type zeolite Y (HY) at a Al/Si weight ratio of 0.36. Both of the surface modified and unmodified HY powders were used as supports for nanogold in this study. The procedures of surface modification on HY are as follows: a desired amount of zeolite powders was placed into 1 N $NaNO_{3(aq)}$ solutions and maintained at 30 °C. The solution pH was adjusted to 6 by adding 1 N $NaOH_{(aq)}$. After three hours of pH adjustment, the zeolite-suspended solutions were filtered. The filter cakes without any washing were dried at room temperature. The resulting HY is named "H(Na)Y". On the other hand, the filter cakes which had been washed with large amounts of de-ionized water after the filtration and were dried at room temperature is named "H(Na)Y-w".

2.2. Preparation of Au/Y catalysts

The procedures for preparing Au/Y are as follows: First, 1.6×10^{-3} M chloroauric acid ($HAuCl_4 \cdot 3H_2O$) solution was prepared and maintained at 30 °C. 1 N $NaOH_{(aq)}$ was added dropwise into the solutions to adjust pH to be steady at 6 for 4 h. Then, a suitable amount of zeolite powders were added into the solutions. Re-adjustment of solution pH was needed if pH deviated from 6 substantially after adding zeolite powders into the solutions. For Au/Y with modified HY (such as H(Na)Y and H(Na)Y-w) as supports, re-adjustment of solution pH was not needed because the pH of Au solutions was only slightly above 6 after adding zeolite powders into the solutions.

Then, the suspension was heated to 80 °C and maintained for 1 h. After cooling down to room temperature, the suspensions were filtrated. The filter cakes were washed with large amount of de-ionized water to remove residual Cl as much as possible. Finally, they were dried at room temperature and stored in a sealed glass vial covered with black tape, for preventing the sample exposed to light. The prepared Au/Y with HY as the support is named "Au/HY", and the Au/Y with surface-modified HY (*i.e.*, H(Na)Y and H(Na)Y-w) as supports are named "Au/H(Na)Y" and "Au/H(Na)Y-w", respectively.

For comparison, another Au/Y was prepared following the preparation procedures of Okumura *et. al* [18]. In their procedures, $HAuCl_4$ solutions at a concentration of 1.6×10^{-3} M were prepared and maintained at 70 °C. Then, HY powders were added into Au solution, followed by addition of 2.8% ammonium solutions into the suspensions to adjust pH to be steady at 6. Then, the suspension was filtered and the filter cake was washed with large amounts of de-ionized water. This sample is named "Au/HY-pH2"because the pH of Au solution was at *ca.* 2.6 before the addition of zeolite powders. It should be emphasized that the discrepancy in the preparation between Au/HY-pH2 and other samples lies in the timing of adjusting pH. In this case, pH was adjusted to 6 after zeolite powders were added into Au solutions. As to other samples, pH has been adjusted to 6 before the addition of zeolite into Au solutions.

2.3. Activity tests for CO oxidation

CO oxidation was carried out in a quartz tube reactor at 25 °C under atmospheric pressure. The total volumetric flow rate to reactor inlet was 99 mL/min, containing 1 vol% of CO and 99 vol% of air. By passing through a water trap at 0 °C, the gas flow was saturated with water vapor at a concentration of 6000 ppm. Au/Y containing 0.2 mg Au was used for each catalysis test. Shimadzu GC-14A gas chromatograph was used for analyzing the outlet stream. A Carboxen™ −1000 column was applied for separation of carbon dioxide, carbon monoxide, nitrogen and oxygen.

2.4. Characterizations

The Au loading of respective Au/Y were determined by AAnalyst200 atomatic analyzer (AA); other elements like Al and Si were measured by using inductively coupled plasma-mass spectrometer (ICP-MS) with SCIEX ELAN 5000 ICP-MS. Before the measurement by AA and ICP-MS, the prepared Au/Y powders were immersed in HF and Aqua regia until complete dissolution. The surface compositions and oxidation state of atoms were characterized using X-ray photoelectron spectroscopy (XPS) with an ESCALAB 250XPS spectrometer equipped with an Al Kα monochromated X-ray source running at 200 W. Before measurement, the powder samples were mounted on double-sided adhesive tape. The spectra were collected at a dwell time of 50 ms, a pass energy of 20 eV, and steps of 100 meV. Binding energy was referenced to the C 1 s set at 284.5 eV, from the adventitious carbon. The peaks were analyzed by using Avantage v 2.26 after background subtraction, based on a nonlinear least-squares fitting program according to Shirley [29]. High-resolution transmission electron microscopy (HRTEM) photographs were taken with a JEOL JEM-3000F electron microscope operated at 300 kV. Prior to the measurement, the Au/Y powders were suspended in ethanol solutions, and vibrated by sonic oscillation to make the solid powders evenly dispersed. A 200-mesh cupper grid coated with lacey carbon films was used for supporting Au/Y powders. The zeta potential of zeolite powders was measured by using Malvern Nano-ZS. In a typical pretreatment for the measurement, 0.05 g of zeolite powder was mixed with 9 g of deionized water, and the solution was shaken for a good suspension. It was then centrifuged and the upper and clear portion containing the suspended powders was used for the immediate measurements. The average value of zeta potential, obtained from three measurements within 2 min, was adopted. The reduction temperature of Au/Y was detected by using temperature programmed reduction (TPR) apparatus with micromeritics Auto Chem II. The carrier gas was a mixture of 90 vol.% argon and 10 vol.% of hydrogen and the flow rate was 30 mL/min. The temperature of the reactor was raised

Table 1
Zeta potential of supports, preparation conditions, average Au particle size, Au loading, and % of gold in the solutions loaded onto supports for respective Au/Y.

sample	zeta potential of supports (mV)	zeolite/Au solutions ratio(g/mL)	Average Au particle size[c] (nm)	Au loading (wt.%)	% of Au in solutions loading onto supports
Au/HY	-34.4 ± 7.8[a]	1.2/115	2.81	1.16	48.7
Au/H(Na)Y	35.5 ± 0.7[a]	1.2/115	1.74	1.25	51.7
Au/H(Na)Y-w	-10.8 ± 3.2[a]	1.0/115	1.76	0.64	30.0
Au/HY-pH2	10.2 ± 1.1[b]	1.6/115	1.57	1.53	85.6

[a] Zeta potential of zeolite powders were measured in the de-ionized water.
[b] Zeta potential of zeolite powders were measured in aqueous solutions maintained at pH 2.6.
[c] Measured from HRTEM image.

at a rate of 10 °C/min from room temperature to 700 °C. Au L_{III}-edge X-ray absorption near edge structure (XANES) spectra were collected using the transition mode at the beam lines 17C of the National Synchrotron Radiation Research Center (NSRRC) facility in Hsinchu, Taiwan. Standard operating condition was 1.5 GeV and 350 mA. The photon energy was guided using a fixed-exit double-crystal Si(111) monochromator and calibrated with a metallic Au foil (L_{III}-edge, 11 919 eV).

3. Results and discussion

3.1. Zeta potential of HY supports

Table 1 gives the zeta potentials and loadings of gold on various HY zeolite. The zeta potential of fresh HY was −34.4 mV and it reversed to 35.5 mV (*i.e.*, of H(Na)Y) after the surface modification. A washing step on the filter cake of modified HY returned the zeta potential back to negative at −10.8 mV (*i.e.*, of H(Na)Y-w). The reversal of zeta potential is due to desorption of sodium cations from H(Na)Y zeolite. A decrease in zeta potential of H(Na)Y-w is consistent with a decline in sodium contents [28]. Note, despite a negative zeta potential of H(Na)Y-w, it is still higher than that of unmodified HY (*i.e.*, −34.4 mV). It could be due to an uneven distribution of positive charge on H(Na)Y-w sample. To understand the surface charge of HY at the moment zeolite supports were added into solutions in preparing Au/HY-pH2, its zeta potential was measured in a solutions at the same pH as $HAuCl_{4(aq)}$ (*i.e.*, 2.6). The zeta potential was found to be 10.2 mV. One expects $HAuCl_4$-derived gold complexes with negative charge can be loaded onto supports more easily owing to the positive surface charge.

3.2. Au loading amounts on the prepared Au/Y

Nanogold derived from $HAuCl_4$ were loaded onto zeolite samples including HY, H(Na)Y and H(Na)Y-w with various zeta potentials. From Table 1, the Au loading on the fresh HY with zeta potential at −34.4 mV was 1.16 wt.%. As to H(Na)Y at 35.5 mV, the gold loading was 1.25 wt.%. It seems little changes were resulted on Au loading despite the discrepancies in zeta potentials. In fact, nanogold can be deposited onto zeolite supports either by chemisorption with dehydration between hydroxyl groups between gold complexes and zeolite surface or physisorption with electrical attraction. The similarity in Au loading between Au/HY and Au/H(Na)Y can be the consequence of high loading temperature (*i.e.*, 80 °C), under which both of chemisorption and physisorption may simultaneously occur. To focus on the influences of surface charge of supports on Au loading (*i.e.*, physisorption), another samples of Au/HY and Au/H(Na)Y were prepared at lower temperature (*i.e.*, 30 °C). From Table S1, the Au loading of Au/HY dropped to 0.43 wt.%, and that of Au/H(Na)Y dropped to 0.96 wt.%. The Au loading of Au/H(Na)Y is two time higher than that of Au/HY at low temperature, indicating that gold species can be more easily loaded onto supports when the surface charge of supports was reversed to positive.

For H(Na)Y-w with zeta potential at −10.8 mV, the gold loading was 0.64 wt.%. In comparison to the Au loading of Au/H(Na)Y at 1.25 wt.%, the results reveal that fewer Au species can be loaded onto supports as surface charge of modified HY becomes negative. Nevertheless, the Au loading of Au/H(Na)Y-w is even lower than that of Au/HY (*i.e.*, 1.16 wt.%), despite a more positive zeta potential of H(Na)Y-w than that of HY. Previous investigation on gold loadings in Au/HY and Au/H(Na)Y indicates that chemisorption is the dominating mechanism for Au to load onto fresh HY with negative zeta potential. The protons on HY can accelerate the dehydration processes between Au-OH and Si-OH on zeolite surface, inducing high Au loading.

For Au/HY-pH2 prepared under acidic conditions, the zeta potential was found to be 10.2 mV in aqueous solutions with the same pH as that of $HAuCl_{4(aq)}$. The Au loading of resulting catalyst was 1.53 wt.%. It can be found that over 80% of gold species in the solutions could be loaded onto the supports, in comparison to roughly 50% or less for the other samples. The differentiation of Au species in solution depends on the pH condition. At pH = 6, the dominant gold complexes include $Au(OH)_3Cl^-$ and $Au(OH)_3$. $Au(OH)_3Cl^-$ remains monomeric while $Au(OH)_3$ can easily aggregate to form precipitates [30,31]. On the other hand, the dominant complex under pH = 2.6 is the anionic $AuCl_4^-$. The high Au loading for Au/HY-pH2 demonstrates that most of gold complexes in the solutions can be easily loaded onto zeolite by electrical attraction.

3.3. Analyses of Au particle sizes on the prepared Au/Y

In order to understand the sizes of deposited gold nanoparticles and their correlation to catalytic activities, HRTEM micrographs of each sample are taken. The results of Au/HY are shown in Fig. 1(a) and (b). It can be found that gold nanoparticles are evenly dispersed on the supports. From gold particle size distribution presented in Fig. S1(a), most of gold species are larger than the diameter of cages of faujasite structure (*i.e.*, 1.2 nm). They should be located on the external surface of zeolite Y. HRTEM micrographs of Au/H(Na)Y sample are shown in Fig. 1(c) and (d).Very small nanogold particles with sizes *ca.* 1 nm are widely dispersed on the supports. From particle size distribution presented in Fig. S1(b), about 50% of gold species are smaller than 1.2 nm, and 40% are with sizes between 1.2 and 2 nm. It is believed that most of them are either inside the supercage of zeolite Y or partially embedded into the cages. Meanwhile, a few gold nanoparticles with sizes as large as 10 nm can be found on the external surface in Fig. 1(d). The discrepancies in gold size distribution between Au/HY and Au/H(Na)Y suggests that the positive surface charge of modified HY leads to a finer dispersion of gold nanoparticles, whereas the negative surface charge of fresh HY prevents negative gold monomers from loading onto supports. Thus, initial gold species on Au/HY should be mostly $Au(OH)_3$ precipitates and subsequent dehydration and de-oxygen will result in lager Au particles.

The micrographs of Au/H(Na)Y-w are shown in Fig. 1(e) and (f). Very small gold nanoparticles are found finely distributed on the supports with occasional nanoparticle with sizes above 10 nm.

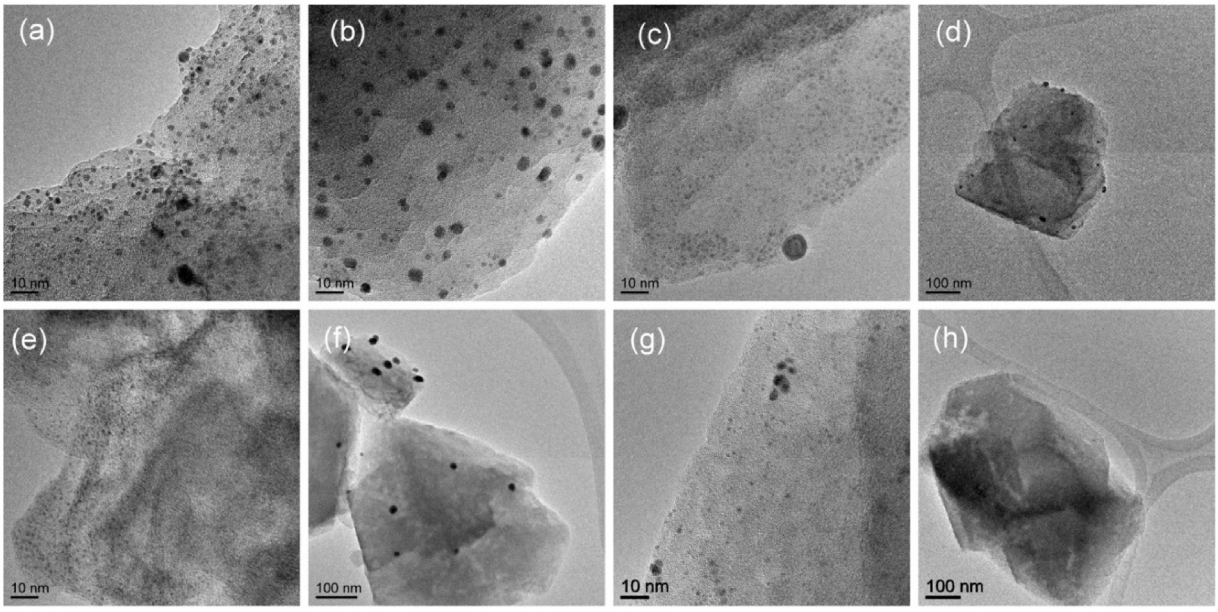

Fig. 1. HRTEM photographs of fresh (a)(b) Au/HY, (c)(d) Au/H(Na)Y, (e)(f) Au/H(Na)Y-w, and (g)(h) Au/HY-pH2.

Despite a lower percentage of gold species below 1.2 nm than those on Au/H(Na)Y, there are still up to 30% of gold nanoparticles smaller than the cage diameters. Gold species on both Au/H(Na)Y and Au/H(Na)Y-w are with sizes extremely small (*ca.* 1 nm) and with those as large as above 10 nm. The similar pattern in size distribution seems contradictory to the discrepancies in zeta potentials (*i.e.*, 35.5 mV for H(Na)Y vs. −10.8 mV for H(Na)Y-w). However, the residual sodium on H(Na)Y-w and abundant Al species around the exterior imply the existence of local positive charge on its surface [28], as evidence by a more positive zeta potential than that of unmodified HY. Accordingly, very small nanoparticles widely dispersed on Au/H(Na)Y and Au/H(Na)Y-w should be mostly resulted from the deposition of negative gold monomers onto positive-surface-charge zeolite supports through electrical attraction. Meanwhile, big nanoparticles with sizes above 10 nm, as observed in Fig. 1(d) and (f), should be due to the $Au(OH)_3$ precipitates. Previous report by Turner et al. emphasized the substantial role of nanogold with sizes near 1 nm as active sites [32]. The samples showing wide dispersion of very small nanoparticles (*ca.* 1 nm) on both Au/H(Na)Y and Au/H(Na)Y-w (Fig. 1(c) and (e)) suggest high catalytic activity.

The HRTEM micrographs of Au/HY-pH2 are shown in Fig. 1(g) and (h). In contrast to other Au/Y, fewer particles can be found on this sample. Most of them are extremely small, even though some large particles (*ca.* 3–4 nm) can be still observed. Fig. 1(h) and statistical analysis on gold particles sizes (Fig. S1(d)) shows no giant particles with sizes above 10 nm, indicating very few $Au(OH)_3$ precipitates. The average gold particle size is the smallest among all the samples (i.e., 1.57 nm in comparison to 1.76, 1.74 and 2.81 nm of the other samples, listed in Table 1). Meanwhile, its standard deviation is the smallest as well (only 0.70 nm in comparison to near 2 nm of the others), showing that gold sizes on Au/HY-pH2 are the most monodispersed. From the viewpoint of preparation conditions, the pH of gold solutions in preparing Au/HY-pH2 was maintained at *ca.* 2.6 before zeolite powders were added into the solutions. It means $AuCl_4^-$ are the dominant solution species before the addition. The absence of large $Au(OH)_3$ precipitates on Au/HY-pH2 indicates that most of negative monomers should have been loaded onto the supports despite the following adjustment of solution pH to above 6, suitable for the formation of $Au(OH)_3$ precipitates. However, it is interesting to notice that fewest amounts of gold particles on this sample can be observed by HRTEM, which seems contradictory to its highest Au loading from AA measurement. The gold particles can be either too small to be found or too deeply deposited (in the cages) to be detected.

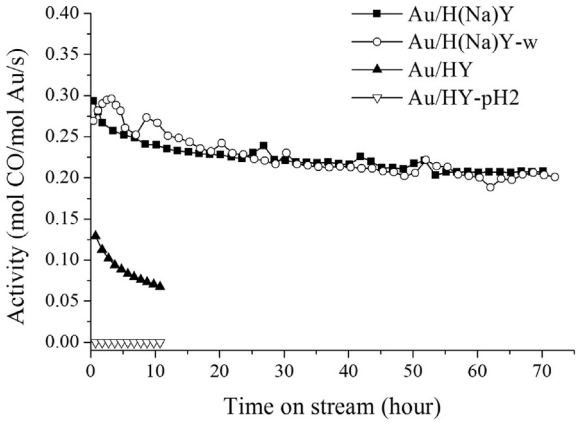

Fig. 2. CO oxidation tests over Au/H(Na)Y, Au/H(Na)Y-w, Au/HY and Au/HY-pH2 at 25 °C. Total volumetric flow rate is 99 mL/min, containing 1 vol.% of CO and 99 vol.% of air. Au/Y catalysts containing 0.0002 g Au were used for activity tests.

3.4. Room-temperature CO oxidation tests

All the samples were tested in catalytic CO oxidation at 25 °C. The results are shown in Fig. 2. It can be found that an initial rate of CO oxidation for Au/HY was found at 0.13 mol CO/mol Au·s and it decayed continuously with increasing time on stream. After 10 h, only a rate of 0.07 mol CO/mol Au·s was left (54% of initial reactivity). On the other hand, an initial activity for Au/H(Na)Y started from a higher CO conversion at 0.3 mol CO/mol Au·s and decreased with increasing time on stream. The decay rate was apparently lower than that for Au/HY. After 40 h of reaction, it became stable at *ca.* 0.21 mol CO/mol Au·s and maintained the same activity until the end of reaction. Roughly 70% of initial activity was retained. In comparison to Au/HY, higher activity was obtained from Au/H(Na)Y. Stable performance in a long-term test was found as well. This is in accordance with the HRTEM images showing smaller sizes and

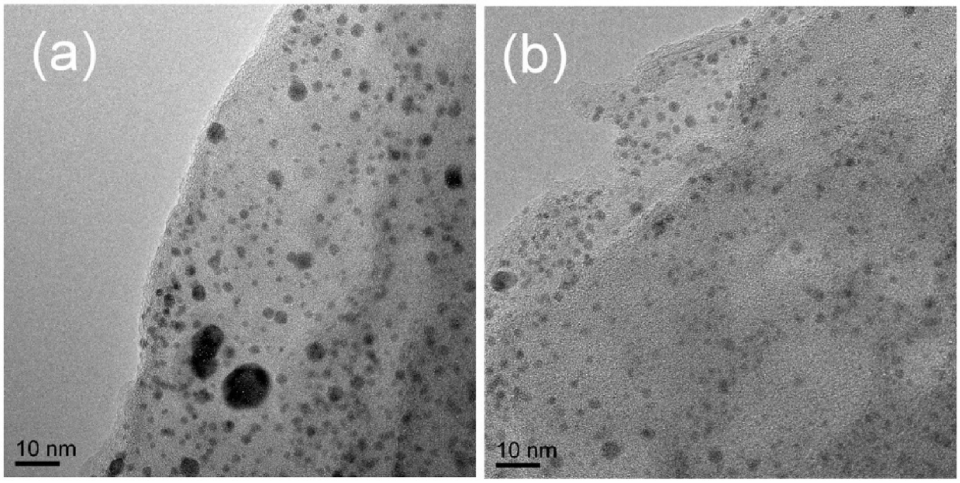

Fig. 3. HRTEM photographs of reacted Au/H(Na)Y.

finer dispersion of gold nanoparticles on Au/H(Na)Y than those on Au/HY.

As to Au/H(Na)Y-w, it is interesting to notice that its catalytic performance is quite close to that of Au/H(Na)Y. It started from *ca.* 0.27 mol CO/mol Au·s, and became stable at 0.2 mol CO/mol Au·s after 40 h of reaction. The similarity in the catalytic performances between Au/H(Na)Y and Au/H(Na)Y-w is consistent with their similar characteristics in gold particle sizes as well as their preferred spatial distribution near external surface (will be shown in Table 2). From HRTEM micrographs in Fig. 1(c) and (e), finely dispersed gold nanoparticles can be found on both samples, with their sizes as small as 1 nm. In fact, gold species around 1 nm or less, as confined in supercage, are considered catalytically more active, as reported by Turner et al. and Herzing et al. [32,33].

Finally, Au/HY-pH2 shows no activity during a 10-h reaction test in CO oxidation. It turns out the Au/Y with the smallest gold particles (listed in Table 1) presents the lowest catalytic activity for CO oxidation. It should be due to the potential contents of residual Cl, owing to a lower pH during the preparation (relevant evidences will be presented in sections 3.6). As a matter of fact, a high temperature pretreatment in 10 vol.% H_2/N_2 flows (at 127 °C) was able to activate the catalyst (Fig. S3), as reported in the research work from Okumura et al. [18]. The residual Cl are supposed to be removed through the reaction with H_2 to from HCl. However, the activity of pretreated catalyst decayed drastically despite improved activity. Severe aggregation of gold species was found after the high-temperature pretreatment (Fig. S4) and thus explain the severe decline of activity. Similar phenomena were observed on Au/H(Na)Y-w (as a reference) after the same pretreatment in H_2/N_2 flows (Fig. S3 and S4).

3.5. Analyses of Au particle sizes on the modified Au/Y after CO oxidation

A comparison study of Au/H(Na)Y before and after CO oxidation was carried out to find out the correlation between the change in gold particle size and its activity performances. Fig. 3 shows the HRTEM micrographs of reacted Au/H(Na)Y. Nanogold with sizes above 2 nm are indicated in Fig. 3(a). Some of them are even larger than 5 nm. Meanwhile, there are still abundance of particles with size in the range between 1 ~ 2 nm, as shown in Fig. 3(b). To understand the size change in a statistical way, a plot of particle size distribution is shown in Fig. S2. In comparison to those on fresh Au/H(Na)Y, it can be found that gold species below 1.2 nm decreases from roughly 50% to near 10% after the reaction. Meanwhile, those in the range between 1.2 and 2 nm increase from ~40% to above 50%. Those in the range of 2–3 nm and 3–4 nm are found increased as well. It is interesting to find that the amounts of particles with sizes above 5 nm decrease after the reaction, indicating decomposition of most $Au(OH)_3$ precipitates during CO oxidation. In general, the average size of gold particles increases from 1.7 to 2.0 nm, which means gold sintering is evident after CO oxidation.

Nevertheless, there are still 10% of gold species smaller than the diameter of supercage (i.e., 1.2 nm). These ultrasmall particles are considered catalytically active, as found from Herzing et al. and Turner et al. [32,33]. Meanwhile, it can be found that over half of gold species on reacted Au/H(Na)Y are between 1.2–2 nm. They are only slightly larger than inner spaces of supercage (i.e., 1.2 nm) and demonstrate limited size growths after the reaction. It is considered that the gold particles on the exterior surface can be anchored on the pores through collision with those confined inside cages. Thus, these outer particles became less dynamic and hardly move around and sinter with other particles. The limited size growth corresponds to a stable activity in a long-term reaction as well as high activity.

3.6. Analyses of Au deposition sites and Al species on the prepared Au/Y

To understand the deposition of nanogold on respective Au/Y samples, characterization methods including AA, ICP and XPS were used. Recent work investigating the effect of surface modification on the zeta potential of HY has found that the reversal of surface charge of HY zeolite is accompanied with diffusion of extra-framework Al to the exterior surface [28]. To understand how these Al species affect the deposition of nanogold on zeolite supports, both Al and Au distributions around each Au/Y sample were investigated.

Table 2 shows the weight ratios of Al/Si and Au/Si in the bulk and on the exterior surface. According to the results, the bulk Al/Si weight ratios were found to be 0.34, 0.39, 0.34 and 0.33 for Au/HY, Au/H(Na)Y and Au/H(Na)Y-w and Au/HY-pH2, respectively. Differences between them are insignificant. They can result from either measurement errors (standard deviation of 0.03 according to 5-time measurements over the same sample) or a slight removal of Al or Si species during the preparation. On the other hand, the exterior Al/Si ratios were found to be 0.49, 1.16, 1.26 and 0.47. High exterior Al/Si ratios were found on Au/Y with surface modified HY as the supports, indicating an abundance of Al species around the exterior regions. This is in accordance with a high content of surface Al on HY after the modification [28].

Table 2
Au loading and elementary analyses in the bulk and on the exterior surface of Au/HY, Au/H(Na)Y, Au/H(Na)Y-w and Au/HY-pH2.

sample	Au loading(wt.%)	Overall (by AA, ICP)		Surface (by XPS)		(Au/Si)XPS/(Au/Si)ICP, AA
		Au/Si	Al/Si	Au/Si	Al/Si	
Au/HY	1.16	0.049	0.34	0.28	0.49	5.71
Au/H(Na)Y	1.25	0.055	0.39	0.89	1.16	16.06
Au/H(Na)Y-w	0.36	0.014	0.34	0.23	1.26	16.43
Au/HY-pH2	1.53	0.058	0.33	0.13	0.47	2.25

On the other hand, the bulk Au/Si weight ratios were found to be 0.049, 0.055, 0.014 and 0.058for Au/HY, Au/H(Na)Y, Au/H(Na)Y-w and Au/HY-pH2, respectively. The values are proportional to the Au loading of respective sample. Meanwhile, the exterior Au/Si ratios on each sample were 0.28, 0.89, 0.23 and 0.13. Owing to different amounts of loaded Au, the large value in exterior Au/Si ratio does not necessarily mean higher proportion of total gold on the exterior surface. Therefore, these values were standardized via dividing the exterior Au/Si ratios by bulk Au/Si ratios, as indicated by the coefficient of $(Au/Si)_{XPS}/(Au/Si)_{ICP,AA}$ in Table 2. They transferred to 5.71, 16.06, 16.43 and 2.25 for Au/HY, Au/H(Na)Y, Au/H(Na)Y-w and Au/HY-pH2, respectively. Higher ratios were obtained for both of surface modified HY supported nanogold catalysts (*i.e.*, Au/H(Na)Y and Au/H(Na)Y-w), while lower ratios were found for the other samples with unmodified HY as the supports. It means nanogold on modified HY are more exteriorly distributed, whereas those on fresh HY more interiorly embedded. This result can be correlated to the distribution of Al species because higher exterior Al/Si ratios are also found for modified samples (*i.e.*, Au/H(Na)Y and Au/H(Na)Y-w) whereas lower ratios are observed for Au/Y with unmodified HY as supports. It seems these Al species can attract nanogold to deposit aside. According to our recent study [28], the increment of Al species are evidently found after the surface modification and can induce charge reversal in zeta potential in synergy with adsorbed sodium cations. This implies positive charge on these sites and enables electrical attraction with negative gold complexes during preparation.

In correlation to HRTEM photographs, the lower $(Au/Si)_{XPS}/(Au/Si)_{ICP,AA}$ ratio for Au/HY-pH2 is consistent with the corresponding images showing fewer amount of gold nanoparticles (Fig. 1(g) and (h)), implying that gold species on this sample are deposited too deeply within the support as seen by HRTEM. Hard accessibility of gold active sites to reactant gas during catalysis is suggested. On the other hand, high $(Au/Si)_{XPS}/(Au/Si)_{ICP,AA}$ ratios were obtained for both of modified samples (*i.e.*, Au/H(Na)Y and Au/H(Na)Y-w), implying that most of gold species are deposited on the outer surface. From HRTEM micrographs, shown in Fig. 1(c) and (e), one can see their sizes are extremely small. Most of them are even smaller than the cage diameter of zeolite Y (*i.e.*, 1.2 nm). Thus, these gold species are supposed be accommodated inside the cages, with their positions close to the outer surface and under a depth detectable by XPS (*ca.* 5 nm). From the catalytic results as shown in Fig. 2, the activities of both Au/H(Na)Y and Au/H(Na)Y-w are high. This is ascribed to their small sizes of gold particles, as well as the preferred spatial distribution near external surface. From the viewpoint of internal mass transfer, these exteriorly deposited gold active sites are more accessible to reactant molecules than those embedded deep inside the zeolite, and thus enable higher activities.

3.7. Analyses of residual Cl on the prepared Au/Y

According to Oh et. al., Cl has been proven to be the cause of sintering of gold nanoparticles [20]. In this study, the low solution pH in preparing Au/HY-pH2 implies a high content of residual Cl. Despite a post adjustment of solution pH to 6 after addition of zeolite powders into gold solutions, it is not certain if the attached Cl on Au centers can be replaced by hydroxyl groups once gold monomers have deposited onto supports. Thus, characterizations including XANES and XPS measurements were used to investigate the amounts of residual Cl, as well as TPR to differentiate the categories of gold cations on Au/Y.

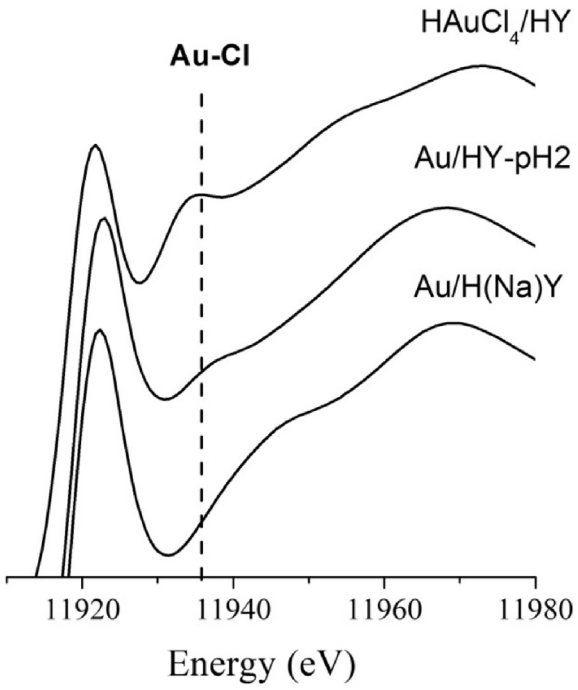

Fig. 4. Au L_3-dge XANES spectra of $HAuCl_4$/HY, Au/HY-pH2 and Au/H(Na)Y.

Au L_3-edge XANES spectra are shown in Fig. 4. A reference sample named $HAuCl_4$/HY was prepared by loading $AuCl_4^-$ species onto HY supports via incipient wetness impregnation. The intense peak at 11936 eV is assigned to Au—Cl bond [18]. From the spectra of Au/HY-pH2, a broad band was found at the same eV, whereas no intensity was found on Au/H(Na)Y. This demonstrates a higher content of residual Cl in Au/HY-pH2 than those in Au/H(Na)Y. On the other hand, XPS spectra of Cl 2p are shown in Fig. 5. No peak was found on Au/HY-pH2, whereas a small intensity was observed on Au/H(Na)Y. It means there is trace Cl on Au/H(Na)Y, and can be the cause for initial decay of activity as observed in the reaction tests (Fig. 2). However, no peak of Cl 2p on Au/HY-pH2 XPS spectrum seems contradictory to the evident band at 11936 eV shown in XANES result (Fig. 4). It means most of Cl in Au/HY-pH2 are deposited inside bulk catalyst, whereas few Cl are found on the exterior surface. In correlation to the spatial distribution of Au, nanogold on Au/HY-pH2 are also deeply embedded as indicated by its low $(Au/Si)_{XPS}/(Au/Si)_{ICP,AA}$ ratio. The coincidence in the spatial distribution of Cl and Au suggests the presence of Cl-attached gold species.

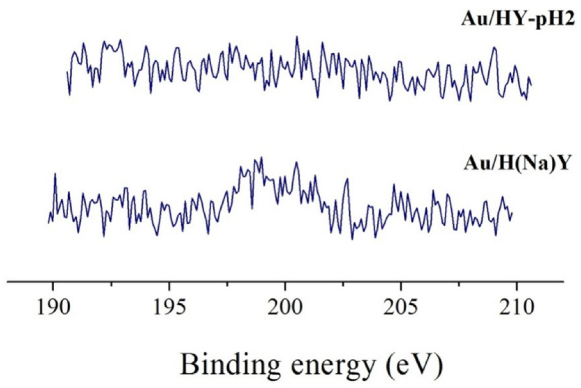

Fig. 5. XPS Cl 2p spectra of Au/HY-pH2 and Au/H(Na)Y.

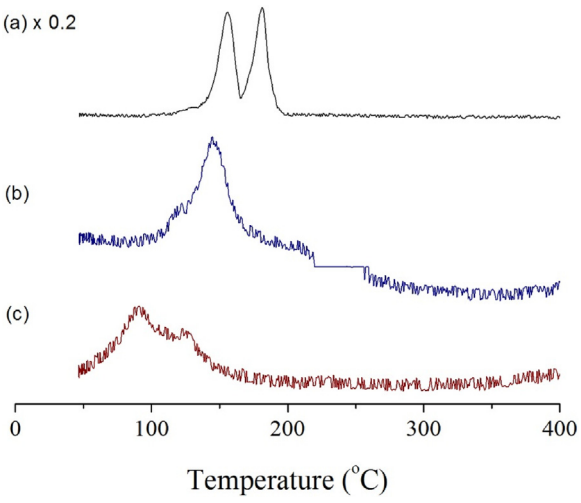

Fig. 6. TPR spectra of (a) $HAuCl_4$/HY, (b) Au/HY-pH2 and (c) Au/H(Na)Y.

3.8. Valence and temperature programed reduction behaviors

Because cationic gold are found on all Au/Y samples from XPS Au 4f spectra, temperature programed reduction (TPR) was used to study the reductions under hydrogen to differentiate the gold species on various samples. In comparison, a $HAuCl_4$/HY sample was also studied to specify the reduction temperature of $AuCl_4^-$ species. From Fig. 6(a), the spectrum of $HAuCl_4$/HY show two distinct peaks, one at 155 °C and the other at 181 °C. They are assigned to the reductive removal of Cl in $AuCl_4^-$ complexes at two different steps. On the other hand, the peak in Au/HY-pH2 spectra is located at 145 °C, with a broad band extended to higher temperature. Meanwhile, a small shoulder appeared at *ca.* 120 °C as well (Fig. 6(b)). Note, the peak in Au/HY-pH2 spectrum is quite close to the first peak in $HAuCl_4$/HY spectrum, implying a high content of $AuCl_4^-$. This shows that Au—Cl bond is mainly present in coordination of Au in this catalyst. This agrees well with the high Cl content detected by XANES in Au/HY-pH2.Meanwhile, the shoulder appeared at lower temperature indicated the existence of Au—O bonds as well, showing that there can be still partial replacement of chloride with hydroxyl groups during preparation when basic liquids were dropped into the solutions after dispersing HY into gold solutions. On the other hand, a reduction peak at 91 °C and a broad shoulder near 125 °C are found in Au/H(Na)Y spectrum. The reduction peak at lower temperature is assigned to Au(III) species with Au—O bond. The shoulder at higher temperature side(125 °C) is perhaps due to more stable Au—O on larger particles located on the exterior surface [34]. We also examined the distribution of valences

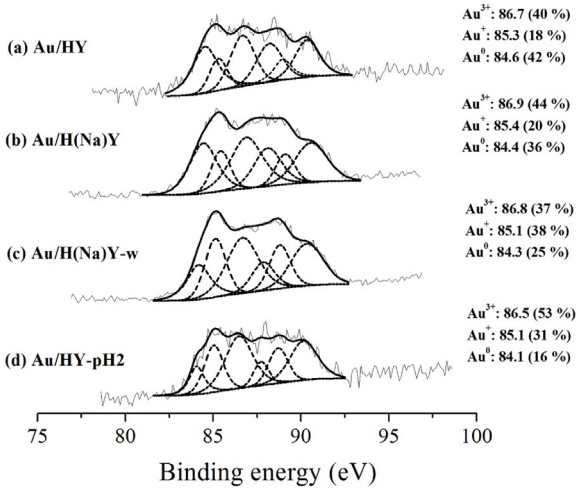

Fig. 7. XPS Au 4f spectra and deconvolution results of (a) Au/HY, (b) Au/H(Na)Y, (c) Au/H(Na)Y-w and (d) Au/HY-pH2.

of gold species in all the samples by XPS Au 4f spectra (Fig. 7). One can see that all catalysts possess high content of oxidized gold (Au(I) and Au(III)) which is consistent with the TPR result in Fig. 5(c). This mixed form of Au(0) and oxidized Au on Au/H(Na)Y is resulted from our unique synthesis procedure where no high temperature treatment or reduction of our catalysts are executed for removing oxygen. In contrast, standard deposition-precipitation method always needs some hydrogen reduction [18,19]. in order to activate the catalysts. We also note that after catalysis of CO oxidation, most of the gold species in the catalyst reverted to Au(0) (Fig. S5). This may imply that initial lattice oxygen in Au—O bonding may be involved in the oxidation of CO. For Au/HY-pH2, despite a similar pattern of coexistence of Au(0) and oxidized Au with Au/H(Na)Y, high contents of residual Cl, as found from both TPR and XANES, explains why it shows no activity.

3.9. Comparison study with literature works

In this section, we would like to make comparison with literature reports on the size and catalytic activities of the Au nanoparticle. For the sizes of the Au nanoparticles, we only examine those zeolite-encapsulated Au in literature. Table S2 gives comparison of the sizes of zeolite-encapsulated Au nanoparticles in various reports. Basically, there have been two different approaches of making zeolite-encapsulated Au nanoparticles (i) post-synthesis loadings and (ii) encapsulation during synthesis of zeolite. In approach (i), the loadings of Au species to ready-formed zeolite can be done either by ion exchange of cationic Au species such as $Au(en)^{3+}$(gold(III) ethylenediamine complex) [13] or by precipitation-deposition from $HAuCl_4$ [14]. In either case, some high temperature activation treatment is necessary for removing ligands (ethylene diamine or chloride). Consequently, the size of the Au nanoparticles tends to grow to be bigger (~3 nm) than the size of the zeolite cage. Nonetheless, this method offers good stability of the Au nanoparticles. In co-condensation approach (ii), gold precursors are mixed in the synthesis gel of the zeolite such that gold precursors are encapsulated [26,35]. Subsequent hydrothermal treatment crystalized the zeolite with gold nanoparticles encapsulated within. Approach (ii) generally gave smaller gold nanoparticles in the size of 1–2 nm because of the strong confinement of zeolites (see examples in Table S2). However because of the use of hydrothermal synthesis, one needs special precursors such as mercaptosilanes [26,35].

Table 3
Comparison of CO oxidation reactivity of Au/H(Na)Y in this study with literature.

Catalysts	Modification on supports	Pretreatment before CO oxidation	Average Au particle size (nm)	Reaction condition		GHSV (mL/g/h)	Activity (mol CO/mol Au·s)	Ref.
				Temp. (°C)	Gas compositions (vol.%)			
Au/SBA-15 Au/MCM-series	silane functionalization (APTES, aminopropyl-triethoxysilane)	10 vol.% H_2/N_2 flows at 600 °C	5.1	80	CO/air = 1/99	99,000	0.027 (within 1 h)	[15]
Au/SBA-15	silane functionalization (N-trimethoxysilylpropyl N,N,N trimethylammonium chloride)	–	4.5	30–90	CO/air = 1/99	20,000	0.0025[b] (at 90 °C)	[16]
Au/TiO_2	–	H_2 flows at 300 °C	3.2	25	CO/O2/He= 1/9/90	180,000	0.25 (after 1 h)	[37]
Au/HY	–	10 vol.% H_2/N_2 flows at 127 °C	<1.3[a]	0	$CO/O_2/N_2$ = 1/20/79	19,800	0.0098 (within 10 min)	[18]
Au/H(Na)Y	surface modification in $NaNO_3$	–	1.7	25	CO/air = 1/99	297,000	0.21 (after 70 h)	this study

[a] The size is estimated from the coordination number derived from EXAFS fitting.
[b] Variable temperature reaction test.

The special contribution of this work is that we are able to deposit ultrasmall Au nanoparticle of ~1 nm in size in the supercage of zeolite without any high temperature treatment (either hydrothermal, calcination or hydrogen reduction). The ultrasmall Au nanoparticle is extraordinarily active in the catalytic oxidation of CO. Our success in making active Au nanoparticle of such small size may be due to three factors. One is that no organic ligand or chlorides are on the resulting Au nanoparticle and there is no need for any high temperature treatments to remove these ligands. Second is that the strong confinement of the supercage of zeolite Y makes very small sized gold. Third is that de-oxygenation of gold species to Au(0) presumably could occur at room temperature. High activity was found on Au/H(Na)Y on which all gold species were reduced to Au(0) (Fig. S5).

A comparison study with literature work on Au-catalyzed CO oxidation activities was conducted and summarized in Table 3. For organosilane-modified aluminosilicate supported gold catalysts, high-temperature treatments are usually necessary for removing the residual organics and reducing gold cations [15,21,22]. Nevertheless, this could lead to size growth of gold particles. As found in Table 3, gold species on these organosilane modified samples can grow up to ~5 nm. The corresponding activities are at least one-order lower than the activity of surface modified HY supported gold catalysts in this study. Also, their reaction temperatures are all higher than the 25 °C used in this study as well. Meanwhile, the activity of prepared Au/HY as reported from Okumura et. al [18]. is only 0.0098 mol CO/mol Au·s of a very low value, despite a lower reaction temperature (0 °C). Their average size of gold particles is estimated to be below 1.3 nm (which is the smallest in Table 3), based on the coordination number derived from EXAFS fitting. It turns out the preparation methods (i.e., support surface pretreatment and the solution pH for deposition of gold species) can be more crucial to the catalytic activity. Finally, the activity of Au/H(Na)Y (in which aluminosilicate material is an inert support) prepared in this research can be maintained at 0.21 mol CO/mol Au·s even after 70 h of reaction test which is comparable to the activity of Au/TiO_2 (in which TiO_2 is an active support with reducible properties [36]) as reported in the literature [37]. This extraordinarily high activity in CO oxidation was unprecedented in Au supported on aluminosilicates presumably due to the ultrasmall size of the resulting gold nanoparticle.

4. Conclusions

Proton-type zeolite Y (HY) with Al/Si weight ratio at 0.36 was used as supports for loading $HAuCl_4$-dervied nanogold species to prepare Au/Y and used for room-temperature CO oxidation. We found the negative surface charge of HY zeolite can be reversed to positive after a pretreatment with Na^+. In this study we investigate the effect of surface charge of HY zeolite on the supported nanogold catalysts. The activity of nanogold on modified HY (*i.e.*, Au/H(Na)Y) reaches an unprecedentedly high value at 0.21 mol CO/mol Au·s in comparison with Au/HY. According to characterization results, the distinction between Au/HY and Au/H(Na)Y can be summarized as follows. First, Au loading increases as the surface charge of HY supports is reversed to positive. Electrical attraction between negative gold complexes and positive zeolite surface is evidently found. Second, fine dispersion of ultrasmall gold nanoparticle confined in the supercage of zeolite Y (~1 nm) were found on Au/H(Na)Y. In comparison, larger particles were found on Au/HY. Third, gold species on modified HY are more exteriorly distributed than those on fresh HY. From the view point of internal mass transfer in catalysis, an easier accessibility of gold active sites to reactant molecules is suggested. In comparison, lowering the solution pH in preparing Au/Y is able to reverse the surface charge of zeolite supports (*i.e.*, Au/HY-

pH2). However, the resulted high Cl contents can poison the gold active sites and cause deactivations.

We have found a general method to load ultrasmall gold nanoparticle of ~1 nm in the supercage of zeolite Y without any high temperature post treatment and to obtain excellent activity in CO oxidation. This method may be generalized to other microporous zeolites. Such micropore-confined ultrasmall gold nanocluster may open up new catalysis that can possess simultaneous advantages in the extraordinary catalytic activity of ultrasmall gold nanoparticle and the size-exclusion selectivity of zeolite.

Acknowledgments

Financial support from Ministry of Science and Technology of Taiwan and the advices from Professor Soofin Cheng and Mr. Guan-Yu Tung are appreciated. The authors thank Wen-Feng Chang for ICP-MS measurements, Hsiu-Wei Cheng, Jui-Ting Chen and Chien-Cheng Chen for technical supports of XPS, Yi-Jen Yu for HRTEM and Jeng-Lung Chen for XAS.

Appendix A. Supplementary data

Supplementary data associated with this article can be found, in the online version, at http://dx.doi.org/10.1016/j.apcatb.2017.06.083.

References

[1] M. Haruta, Gold Bull. 37 (2004) 27–36.
[2] V. Polshettiwar, R.S. Varma, Green Chem. 12 (2010) 743–754.
[3] V. Ulrich, B. Moroz, I. Sinev, P. Pyriaev, V. Bukhtiyarov, W. Grunert, Appl. Catal. B: Environ. 203 (2017) 572–581.
[4] E. del Rio, A.B. Hungria, M. Tinoco, R. Manzorro, M.A. Cauqui, J.J. Calvino, J.A. Perez-Omil, Appl. Catal. B: Environ. 197 (2016) 86–94.
[5] L. Soler, A. Casanovas, A. Urrich, I. Angurell, J. Llorca, Appl. Catal. B: Environ. 197 (2016) 47–55.
[6] Z. Ma, S. Dai, Nano Res. 4 (2011) 3–32.
[7] M. Kipnis, Appl. Catal. B: Environ. 152–153 (2004) 38–45.
[8] P. Maity, S.H. Xie, M. Yamauchi, T. Tsukuda, Nanoscale 4 (2012) 4027–4037.
[9] Z.L. Wu, G.X. Hu, D.E. Jiang, D.R. Mullins, Q.F. Zhang, L.F. Allard, L.S. Wang, S.H. Overbury, Nano Lett. 16 (2016) 6560–6567.
[10] A. Cao, R. Lu, G. Veser, Phys. Chem. Chem. Phys. 12 (2010) 13499–13510.
[11] Y.M. Kang, B.Z. Wan, Appl. Catal.A: Gen. 128 (1995) 53–60.
[12] A. Pestryakov, I. Tuzovskaya, E. Smolentseva, N. Bogdanchikova, F.C. Jentoft, A. Knop-Gericke, Int. J. Mod. Phys. B 19 (2005) 2321–2326.
[13] D. Guillemot, M. PolissetThfoin, J. Fraissard, Catal. Lett. 41 (1996) 143–148.
[14] H. Chen, X.L. Jia, Y.D. Li, C.J. Liu, Y.H. Yang, Catal. Today 256 (2015) 153–160.
[15] Y.S. Chi, H.P. Lin, C.Y. Mou, Appl. Catal.A: Gen. 284 (2005) 199–206.
[16] C.M. Yang, M. Kalwei, F. Schuth, K.J. Chao, Appl. Catal.A: Gen. 254 (2003) 289–296.
[17] M. Okumura, S. Nakamura, S. Tsubota, T. Nakamura, M. Azuma, M. Haruta, Catal. Lett. 51 (1998) 53–58.
[18] K. Okumura, K. Yoshino, K. Kato, M. Niwa, J. Phys. Chem. B 109 (2005) 12380–12386.
[19] J.Y. Cai, H. Ma, J.J. Zhang, Q. Song, Z.T. Du, Y.Z. Huang, J. Xu, Chem. Eur. J. 19 (2013) 14215–14223.
[20] H.S. Oh, J.H. Yang, C.K. Costello, Y.M. Wang, S.R. Bare, H.H. Kung, M.C. Kung, J. Catal. 210 (2002) 375–386.
[21] C.W. Chiang, A.Q. Wang, B.Z. Wan, C.Y. Mou, J. Phys. Chem. B 109 (2005) 18042–18047.
[22] M.T. Bore, H.N. Pham, E.E. Switzer, T.L. Ward, A. Fukuoka, A.K. Datye, J. Phys. Chem. B 109 (2005) 2873–2880.
[23] C.W. Chiang, A.Q. Wang, C.Y. Mou, Catal. Today 117 (2006) 220–227.
[24] M.G. Cutrufello, E. Rombi, C. Cannas, M. Casu, A. Virga, S. Fiorilli, B. Onida, I. Ferino, J. Mater. Sci. 44 (2009) 6644–6653.
[25] X.Y. Liu, C.Y. Mou, S. Lee, Y.N. Li, J. Secrest, B.W.L. Jang, J. Catal. 285 (2012) 152–159.
[26] T. Otto, S.I. Zones, E. Iglesia, J. Catal. 339 (2016) 195–208.
[27] J.N. Lin, J.H. Chen, C.Y. Hsiao, Y.M. Kang, B.Z. Wan, Appl. Catal. B: Environ. 36 (2002) 19–29.
[28] Y.H. Chen, S.J. Huang, B.Z. Wan, Ind. Eng. Chem. Res. 55 (2016) 1921–1928.
[29] D.A. Shirley, Phys. Rev. B 5 (1972) 4709–4714.
[30] E.A. Nechaev, G.V. Zvonareva, Geokhimiya (1983) 919–924.
[31] C.K. Chang, Y.J. Chen, C.T. Yeh, Appl. Catal.A: Gen. 174 (1998) 13–23.
[32] M. Turner, V.B. Golovko, O.P.H. Vaughan, P. Abdulkin, A. Berenguer-Murcia, M.S. Tikhov, B.F.G. Johnson, R.M. Lambert, Nature 454 (2008) 981–983.
[33] A.A. Herzing, C.J. Kiely, A.F. Carley, P. Landon, G.J. Hutchings, Science 321 (2008) 1331–1335.
[34] J.N. Lin, B.Z. Wan, Appl. Catal. B: Environ. 41 (2003) 83–95.
[35] A.B. Laursen, K.T. Hojholt, L.F. Lundegaard, S.B. Simonsen, S. Helveg, F. Schuth, M. Paul, J.D. Grunwaldt, S. Kegnoes, C.H. Christensen, K. Egeblad, Angew. Chem. Int. Ed. 49 (2010) 3504–3507.
[36] X.Y. Liu, A.Q. Wang, T. Zhang, C.Y. Mou, Nano Today 8 (2013) 403–416.
[37] L. Delannoy, R.L. Chantry, S. Casale, Z.Y. Li, Y. Borensztein, C. Louis, Phys. Chem. Chem. Phys. 15 (2013) 3473–3479.